CrossMark

RESEARCH PAPER

Toward numerical prototyping of labs-on-chip: modeling for liquid–liquid microfluidic devices for radionuclide extraction

Gwendolyne Hellé[1] · Sean Roberston[2] · Siméon Cavadias[2,3] · Clarisse Mariet[1] · Gérard Cote[2]

Abstract Liquid–liquid extraction with stratified flows in a rectangular geometry is investigated in a double-Y shape glass chip. The velocity profiles are determined by a numerical method for two chemical systems: U(VI)/HCl/ Aliquat® 336 and Eu(III)/HNO$_3$/DMDBTDMA. These results are compared with the theoretical results obtained from an analytical resolution described in a previous publication. The role of the viscosity difference between the two phases on the hydrodynamics is highlighted, as well as the influence of the geometrical cross section (symmetric and asymmetric channels). The numerical modeling of the mass transfer for the chemical system U(VI)/HCl/Aliquat® 336 was then investigated, taking into account the results derived from the hydrodynamic modeling. Here, an interfacial reaction is assumed, and a global transfer coefficient is determined, enabling the concentration profiles for U(VI) in both the aqueous and organic phases to be obtained. Finally, the comparison between the experimental and theoretical results for different channel lengths allows for the validation of the mass transfer model, as well as a determination of the optimal extraction channel length.

✉ Clarisse Mariet
clarisse.mariet@cea.fr

1 CEA Saclay, DEN/DANS/DPC/SEARS/LANIE,
91191 Gif-Sur-Yvette Cedex, France

2 Chimie ParisTech - CNRS, Institut de Recherche de Chimie
Paris, PSL Research University, 75005 Paris, France

3 UPMC – Univ Paris 06, 4 Place Jussieu, 75005 Paris, France

List of symbols

A	Interfacial area (m^2)
A'	Specific interfacial area (m^{-1})
C	Concentration (mol L^{-1})
$\mathcal{D}_M$	Distribution ratio of M
D	Diffusion coefficient (m^2 s^{-1})
H	Width of the microchannel (m)
h	Position of the interface (m)
I	Identity matrix
K_1	Forward global transfer coefficient (m s^{-1})
K_{-1}	Backward (or revers) global transfer coefficient (m s^{-1})
L	Length of the microchannel (m)
L_{opt}	Optimal microchannel length (m)
n	Normal vector
N	Molar flux (mol m s^{-1})
p	Pressure
p_0	User-defined external pressure
Q	Flow rate (mL h^{-1})
t	Contact time (s)
T	Deviatoric stress tensor
u	Velocity (m s^{-1})
U_0	User-defined initial velocity (m s^{-1})
v	Superficial velocity (m s^{-1})
$\langle v \rangle$	Average superficial velocity (m s^{-1})
W	Depth of the microchannel (m)
V	Volume (m^3)
ρ	Density (kg m^{-3})
μ	Dynamic viscosity (Pa s)
$\%E_M$	Extraction efficiency of M (%)
[]	Concentration (mol L^{-1})

overbar	In organic phase
∇	Divergent operator
DMDBTDMA	N,N'-dimethyl N,N'-dibutyl tetradecylmalonamide
R_4NCl	Aliquat® 336 [$CH_3(C_nH_{2n+1})_3N^+$, Cl^- where $n = 8$ or 10, with $n = 8$ predominating]

Subscripts

eq	At equilibrium
a	In aqueous phase
o	In organic phase
i	Initial
exp	Experimental
max	Maximal
opt	Optimal
th	Theoretical

1 Introduction

Liquid–liquid extraction is of huge importance in radiochemical procedures, as it is extensively used for the purification and concentration of many analytes. However, the disadvantage of this separation technique is that a large amount of organic solvent is needed to dissolve both the extractant and the extracted species. Microfluidic technology is ideally suited for exploitation in solvent extraction due to the intrinsic advantages of the microdimension, i.e., laminar flow conditions, high surface-to-volume ratio, accurate control of reaction time and reduced chemical quantities (Manz and Eijkel 2001; Whitesides 2006). Solvent extraction with stratified flows in a microchannel has started to be applied as a separation technique in the pre-treatment step of the trace metal assay (Tokeshi et al. 2000; Tokeshi and Kitamori 2005) and for some radiochemical applications, as the use of these systems greatly reduces the manipulated volumes, inducing a decrease in both chemical and radiological risks. It includes the extraction of U(VI) in nitric acid media by tributylphosphate in dodecane or in ionic liquids (Hotokezaka et al. 2005; Tsaoulidis et al. 2013a, b), and the extraction of Y, Eu, La (Kubota et al. 2003) or Pr, Nd, Sm (Maruyama et al. 2004) from nitric acid by 2-ethylhexyl phosphonic acid mono-2-ethylhexyl ester (PC-88A) diluted in toluene (Maruyama et al. 2004) or in kerosene (Nishihama et al. 2004, 2006). More recently, the extraction of Am(III) in HNO_3 by *n*-octyl(phenyl)-*N,N*-diisobutylcarbamoylmethylphosphine oxide (CMPO) was studied (Ban et al. 2011). A comparative study of the extraction of Eu(III) from nitric acid by the N,N'-dimethyl N,N'-dibutyl tetradecylmalonamide (DMDBTDMA) and of U(VI) from hydrochloric acid by Aliquat® 336 was performed in the same microchip (Hellé et al. 2012, 2014, 2015). The majority

of the studies were carried out in "Y-junction" glass chips except for the extraction of the radioisotope Cu-64 from an aqueous solution into a toluene solution of 2-hydroxy-4-*n*-octyloxybenzophenone oxime, which was performed in a microfluidic platform fabricated in SIFEL, a moldable perfluoropolyether (Goyal et al. 2014). To date, microfluidic parallel-flow LLE (liquid–liquid extraction) platforms have been made using materials that are compatible with organic solvents and acidic media, i.e., mainly glass.

As a result of this attractiveness, the development of lab-on-chip devices has become a highly competitive field. However, researchers typically do not have the luxury of large amounts of time and money to build and test successive prototypes in order to optimize species delivery, reaction kinetics and/or thermal performances. In contrast to the use of plastics and polymers as fabrication materials, rapid prototyping techniques (Duffy et al. 1998; Ng et al. 2002; Bendsøe and Sigmund 2003) are not enable to cut cost and development time for glass-made lab-on-chips (Wootton et al. 2002; Erickson 2005). To reduce the number of iterations of prototyping, it is all the more important to develop the best design-forecasting methods. Although the initial development of microfluidic devices can be dated to the late 1980s (Tay 2002), study on design methodologies for this area is still relatively immature. In the past, designers have sought to adapt approaches used in other domains (Panikowska et al. 2009). Design methodologies specific to the microdomain have been considered as a necessity, owing to the failure of the application of methodologies used for macrodevices (Albers et al. 2003). Moreover, at the microscale, the main operating forces are viscous forces, interfacial tension, etc, whereas at the macroscale gravity and inertial effects have to be considered (Erickson 2005; Panikowska et al. 2011). Nowadays, numerous studies develop methods of simulation and analysis of chemical processes (Przekwas and Makhijani 2001; Bose et al. 2003; Hisamoto et al. 2003; Vilkner et al. 2004; Erickson 2005; Erickson and Li 2004; Mott et al. 2006; Zhao et al. 2006; Krishnamoorthy et al. 2006; Brennich and Koster 2014), but very few concern hydrometallurgical ones.

Our aim is to develop effective microsystems for the liquid–liquid extraction of radionuclides in analytical procedures using computational and analytical simulation. In a previous study (Hellé et al. 2014), we report the mass transfer behavior of stratified flow in a rectangular microchannel for two chemical systems: a neutral extractant, N,N'-dimethyl N,N'-dibutyl tetradecylmalonamide (DMDBTDMA), for the extraction of Eu(III) from nitric acid, and a liquid anion exchanger, Aliquat® 336, for the extraction of U(VI) from hydrochloric acid, in the same microchip. These two radionuclide extraction systems have not only significant differences in their kinetic behavior, but also possess large variations in the dynamic viscosity ratios

of the two phases (i.e., the solutions of DMDBTDMA are much more viscous than that of Aliquat® 336). A 1D analytical approach was used to provide insight into different parameters which govern the flow velocity profiles. Conditions of flow rates were found to obtain a maximal velocity at the interface and to determine the position of the interface in the microchannel. The model predictions were found to be in good agreement with the experimental results obtained with the two liquid–liquid extraction systems. However, the 1D analytical approach was insufficient to couple simulation of hydrodynamics and mass transfer. Thus, in the present paper, liquid–liquid extraction reactions with these two chemical systems are examined by both analytical and numerical models, focusing on the stratified flow of two immiscible liquids with mass transfer from one phase to another in a rectangular microchannel.

In this work, we provide a basis for selecting the required geometry, leading to stratified flow based on extraction performances. We take advantage of our experimental results to develop and validate mathematical models of the extraction process in parallel flows by investigating the velocity profiles for both the aqueous and organic phases, the influence of the cross-sectional geometry (symmetric, asymmetric) as well as the mass transfer in the microchannel.

The article is organized as follows. After the presentation of the problem in Sect. 2, the model formulation including the description of the governing equations of hydrodynamics used for the two chemical systems and of the mass transfer used for the U/Aliquat® 336 system is detailed in the Sects. 3 and 4, respectively. The present numerical model is compared against experimental data as well as an analytical model in Sect. 5. The article concludes with a summary of the scientific findings and insights gained from the modeling and simulation study (Sect. 6).

2 Problem definition

In this section, we present the microsystem of reference used for the micro liquid–liquid extraction with parallel flows, as well as the two studied chemical systems. Flow rates of the aqueous and organic phases have to be established laminar and parallel to obtain good phase separation at the end of the microchannel and collect each phase separately at the outlets.

2.1 Y–Y shaped microsystem

The geometric parameters of the glass-made microsystems are reported in a previous study (Hellé et al. 2014). It should be noted that for the modeling of both the hydrodynamics and the mass transfer, a rectangular cross section of the microchannel is considered despite the fact that this
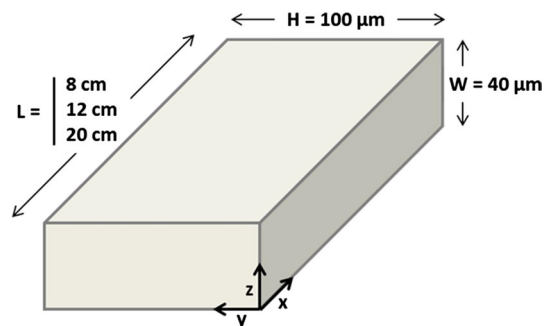

Fig. 1 Geometry of the rectangular cross-sectional microchannel and coordinate system definition for the microsystems ICC-DY10 ($L = 8$ cm), ICC-DY15 ($L = 12$ cm) and ICC-DY200 ($L = 20$ cm)

section is partially rounded in reality (Fig. 1). The uncertainty on the contact times coming from this approximation is less than 10 % according to Ban et al. (2011). Therefore, the 3D geometry used for the modeling is shown in Fig. 1 with the calculation of axis coordinate system (x, y, z). The present modeling focuses on the species transport of the analyte in the main channel. x, y, and z denote the channel's axial, depth-wise, and cross-stream coordinates, respectively.

2.2 Chemical systems

The determination, in batch at the equilibrium, of the optimal chemical conditions for the extraction was performed in a previous study (Hellé et al. 2014) for two chemical systems: Eu(III)/HNO$_3$/DMDBTDMA and U(VI)/HCl/Aliquat® 336. The optimal compositions are [Eu(III)] $= 10^{-2}$ mol L^{-1}, [HNO$_3$] $= 4$ mol L^{-1}, [DMD-BTDMA] $= 1$ mol L^{-1} in n-dodecane and [U(VI)] $= 10^{-5}$ mol L^{-1}, [HCl] $= 5$ mol L^{-1}, [Aliquat® 336] $= 10^{-2}$ mol L^{-1} in n-dodecane modified with 1-decanol 1 % (v), respectively. The physical parameters associated with the two chemical extraction systems used here have been described in a previous study (Hellé et al. 2014). The solution densities and dynamic viscosities were measured using a DMA 4500 density meter (Anton Paar, Austria) and a rotational automated viscosimeter Lovis 2000 M/ME (Anton Paar, Austria), respectively. The extraction performances were then determined for different microchannel lengths.

3 Hydrodynamic behavior

Modeling and simulation analysis (both numerical and analytical) have been actively pursued by numerous researchers to enable a fully resolved view of the unique transport behavior observed in the experiments (Song et al. 2012).

Biphasic segmented flow as well as their typology in microsystems with Y-junctions has been modeled (Rieger et al. 1996; Bird et al. 2007; Jovanovic 2011; Malengier et al. 2012; Malengier and Pushpavanam 2012; Wang et al. 2013; Cherlo et al. 2010; Kashid et al. 2012; Ungerböck et al. 2013; Liu et al. 2014; Lubej et al. 2015). Aota et al. (2007) have proposed an analytical model of interfacial pressure equilibrium for elucidation of the physical mechanism of microcirculation at countercurrent of two immiscible phases in a Y–Y microchannel selectively modified hydrophilic–hydrophobic. Znidarsic-Plazl and Plazl (2009) have made numerical simulations for the flow of two immiscible fluids in a Y-junction microsystem, with the position of the interface centered. A 3D mathematical model for steady-state conditions was developed, comprising velocity profile within the channel, mass transport by convection in the flow direction and diffusion in all spatial directions, as well as equilibrium concentrations at the interfacial areas, which enables accurate process description, and further process optimization was developed for continuous extraction of α-amylase within glass microfluidic chips (Novak et al. 2015). Other authors (Fodor and D'Alessandro 2011) used COMSOL Multiphysics® software for numerical modeling of a gas–liquid biphasic system in parallel within a T-microsystem. Malengier et al. (Malengier et al. 2012; Malengier and Pushpavanam 2012) modeled the hydrodynamics of co-current and countercurrent parallel flows in microchannels with rectangular cross sections. Analytical solutions of aqueous and organic velocity profiles are reported involving fluid flow, viscosity and the geometrical parameters, i.e., the position of the interface and the width H of the microchannel. A numerical relevant resolution prior to the modeling of mass transfer is also proposed. Ranjan et al. (2012) used COMSOL Multiphysics® software for modeling the flows in a Y-junction micromixer. Thanks to the modeling, Stiles and Fletcher (2004) showed that it was possible to control the location of an interface between two immiscible fluids at the exit of a microchannel by adjusting the relative volumetric flow rates of the input stream depending on viscosity.

In this section, we present the governing equations and solutions to velocity profiles of the organic and aqueous phases in microsystems under pressure-driven flow. The analytical 1D model detailed previously (Hellé et al. 2014) has been used here to validate the numerical model of the hydrodynamics. In a second step, a hydrodynamics model coupled with mass transfer is studied.

3.1 Assumptions for the hydrodynamic modeling

The modeling of hydrodynamics requires the resolution of the Navier–Stokes equation to which a few assumptions are implied:

(1) The fluids are newtonian, viscous and incompressible,
(2) There is no effect of the mass transfer or of the chemical reaction on the shape or the volume of the flow or on the position of the interface,
(3) The flow is laminar (low Reynolds number) and in a steady-state,
(4) Bond number is low ($\ll 1$), and the viscous forces are predominant,
(5) The interface is plane.

Based on these assumptions, the laminar flow in the main channel is governed by the steady-state Navier–Stokes equation (Malengier et al. 2011):

$$\frac{\partial p}{\partial x} = \mu \left(\frac{\partial^2 v_x}{\partial y^2} + \frac{\partial^2 v_x}{\partial z^2} \right) \tag{1}$$

3.2 Analytical method

The resolution of linear differential equations can be done analytically, and an exact solution can therefore be achieved. Parabolic velocity profiles are obtained; thus, the flows can be described by Poiseuille-Hagen law, and the velocities are continuous at the interface. The theoretical results predicted for the hydrodynamic modeling with an analytical resolution for the two chemical systems Eu(III)/DMDBTDMA and U(VI)/Aliquat® 336 were presented in a previous article (Hellé et al. 2014).

The analytical resolution offers the advantage of requiring only parameters which can be determined experimentally or which are imposed by the microsystem designer. Nevertheless, the analytical method is limited because it considers only one phase independently of the other, and it takes into account the frictions on the wall parallel to solely the x0z plane.

3.3 Numerical method

For complex geometries or three-dimensional modeling, the analytical method for solving equations may be impossible to use. In this case, the only possibility is to calculate an approximated function using numerical methods. Numerical techniques can be classified into different categories according to the method used for the discretization of the equations (Erickson 2005; Ladeveze 2005). The finite difference solution consists of replacing the partial derivative by a truncated Taylor series based on the values of neighboring nodes (Znidarsic-Plazl and Plazl 2007; Novak et al. 2012; Pohar et al. 2012). This method is easy to implement but it is adapted to the simple geometries (capillaries or sections of channels). With the technique of finite volume, the field of study is divided into a series of controlled

Table 1 Boundary conditions used during momentum transfer calculations, with the governing equation variables being defined as follows: u (velocity), U_0 (user-defined initial velocity), n (normal vector), μ (viscosity), T (deviatoric stress tensor), p (pressure), p_0 (user-defined external pressure) and I (identity matrix)

Boundary type	Boundary condition	Governing equation
Wall	No slip	$u = 0$
Inlet	Velocity	$u = -U_0 n$
Outlet	Pressure, no viscous stress	$\mu(\nabla u + (\nabla u)^T)n = 0$, $p = p_0$
Interior boundary	Continuity	$n(\mu_1(\nabla u_1 + (\nabla u_1)^T) - p_1 I - \mu_2(\nabla u_2 + (\nabla u_2)^T) - p_2 I) = 0$

volumes (2D, triangles, rectangles… and in 3D tetrahedron, hexahedron…) each corresponding to a point on the grid (node) to which the differential equation is integrated (Malengier et al. 2011; Ciceri et al. 2013; Mason et al. 2013). The finite element technique is similar to that of the finite volume except that here, the equations are weighted before being integrated across the field and this method is also suitable for complex geometries (Gervais and Jensen 2006). The choice of numerical modeling will condition the choice of simulation software. A commercial simulation software, COMSOL Multiphysics®, based on the finite element method was used in this study. The interest of a numerical model lies in the extent of its scope, the possibility of taking into account the flows of the two phases simultaneously and coupling phenomena. The main drawback is the need to achieve a fine description of the geometry and parameters.Whatever the numerical method which is chosen, the simplified Navier–Stokes equations are used for the analytical resolution:

$$\nabla.\left(\rho_i vv + p_i I + T\right) = 0 \qquad (2)$$

$$\nabla \cdot v = 0 \qquad (3)$$

All hydrodynamics calculations were done at steady state using the Direct (PARDISO) linear system solver via the COMSOL 3.5a software package. For the momentum transfer studies, the incompressible Navier–Stokes equation was solved using the following boundary conditions (Table 1).

4 Mass transfer

In this section, we present the governing equations and solutions to mass transfer in microsystems under pressure-driven flow. The aim is to use these equations to determine the optimal length of the microchannel for the solvent extraction.

Laminar flow conditions represent one of the main benefits of microfluidics when compared to its macro-scale counterpart. This condition greatly influences the description of diffusion using standard theories such as Fick's law, as inertial forces can be neglected in the dynamics of the mass transfer. The reduction in complexity that this implies allows for basic numerical methods to be used for the modeling (Squires and Quake 2005; Ciceri et al. 2014). In this study, the modeling of the mass transfer has been done only for the chemical system U(VI)/Aliquat® 336 for which the experimental extraction was performed for which the extraction in microsystem was efficient (Hellé et al. 2014), and the interface location centered in the microchannel. It is important to note that the modeling of the mass transfer takes into account the modeling of the hydrodynamics as described previously.

We recall that the extraction of uranium(VI) takes place from 5 mol L^{-1} HCl where it is present as $UO_2(Cl)_4^{2-}$ (Sato et al. 1983).

4.1 Interfacial reaction

Negligible partitioning of Aliquat® 336 into the aqueous phase was assumed (Xu et al. 2003), and the mass transfer modeling was performed considering an interfacial mechanism. Experimentally, the two phases were pre-equilibrated. To simplify the modeling, it has been considered that:

- the Aliquat® 336 does not diffuse in the aqueous phase,
- the aqueous chloro-complex $UO_2(Cl)_4^{2-}$ as an individual species [not as $(R_4N^+)_2 UO_2(Cl)_4^{2-}$] does not diffuse in the organic phase.

The reaction equilibrium is the following (Ryan 1963; Barbano and Rigali 1978; Sato 1983; Razik et al. 1989; Jha et al. 2002; Soderholm et al. 2011):

$$UO_2(Cl)_4^{2-} + 2\overline{R_4N^+, Cl^-} \rightleftharpoons \overline{(R_4N^+)_2 UO_2(Cl)_4^{2-}} + 2Cl^-$$
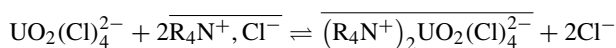
According to the large excess of Aliquat® 336 and Cl$^-$ compared to the uranium(VI) to be extracted ($UO_2(Cl)_4^{2-}$), the concentrations $\overline{R_4N^+, Cl^-}$ and [Cl$^-$] can be considered as constant during the extraction. The kinetics law for this reaction can be written following relation (4), considering a first-order reaction in regard to the uranium(VI) in both the aqueous and organic phases:

$$J_{U(VI)} = K_1[UO_2(Cl)_4^{2-}] - K_{-1}\left[\overline{(R_4N^+)_2 UO_2(Cl)_4^{2-}}\right] \quad (4)$$

Table 2 Physical parameters and initial conditions used for the mass transfer modeling for the chemical system [U(VI)] = 10^{-5} M, [HCl] = 5 M, [Aliquat® 336] = 10^{-2} M, in *n*-dodecane modified with 1-decanol 1 % (v), *(Soderholm et al. 2011), **(Toulemonde 1995)

Parameters	Aqueous phase	Organic phase
$D_{UO_2(Cl)_4^{2-}}$ (m^2 s^{-1})	10^{-8}*	–
$D_{(R_4N^+)_2UO_2(Cl)_4^{2-}}$ (m^2 s^{-1})	–	10^{-9}**
ρ (kg m^{-3})	1081	750
μ (mPa s)	1.27	1.48
Q_{inlet} (m^3 s^{-1})	2.6×10^{-11}	2.3×10^{-11}
Q_{outlet} (m^3 s^{-1})	2.6×10^{-11}	2.3×10^{-11}
v_0 (m s^{-1})	1.39×10^{-2}	1.11×10^{-2}
[$UO_2(Cl)_4^{2-}$] (mol L^{-1})	10^{-5}	–

Table 3 Boundary conditions and associated equations used for the mass transfer modeling for the chemical system [U(VI)] = 10^{-5} M, [HCl] = 5 M, [Aliquat® 336] = 10^{-2} M, in *n*-dodecane modified with 1-decanol 1 % (v)

Boundary	Boundary condition	Equation
Wall	Isolation	$n \cdot N = 0$; $N = -D\nabla C + \vec{v}C$
Inlet	Concentration	$C = C_0$
Outlet	Convective flux	$n \cdot (-D\nabla C) = 0$
Interface	Inward flux	$-n \cdot N = N_0$; $N = -D\nabla C + \vec{v}C$

where $J_{U(VI)}$ refers to the local flux (mol m^{-2} s^{-1}) of $(R_4N^+)_2UO_2(Cl)_4^{2-}$ generated at the interface and directed into the organic phase; the concentrations are per-volume values, located in each phase and adjacent to the interface,

where K_1 (m s^{-1}) and K_{-1} (m s^{-1}) denote the forward and backward global transfer coefficients, respectively.

As at the equilibrium $J_{U(VI)} = 0$, we have merely:

$$\mathcal{D}_{U(VI),eq} = \frac{K_1}{K_{-1}} \tag{5}$$

which denotes the distribution ratio of uranium(VI) at the equilibrium.

Therefore, Eq. (4) can be rewritten as:

$$J_{U(VI)} = K_1\left([UO_2(Cl)_4^{2-}] - \frac{1}{D_{(U(VI),eq}}\left[\overline{(R_4N^+)_2UO_2(Cl)_4^{2-}}\right] \right) \tag{6}$$

According to the experimental results obtained previously (Hellé et al. 2014) at the equilibrium,$\mathcal{D}_{U(VI),eq} = 5.90.5$; thus, it can finally be written:

$$J_{U(VI)} = K_1\left([UO_2(Cl)_4^{2-}] - 0.17\left[\overline{(R_4N^+)_2UO_2(Cl)_4^{2-}}\right] \right) \tag{7}$$

with $\frac{1}{\mathcal{D}_{U(VI),eq}} = 0.17$,

4.2 Modeling specifications

All calculations concerning mass transfer have been made using the COMSOL Multiphysics® direct solver SPOOLES. To limit the number of cells, the geometry has been studied in two dimensions using identical values to those implemented in the experimental microsystems: $L = 8$, 12 or 20, $H = 100$ μm with $h = 50$ μm (corresponding to the position of the interface in the microchannel width). The physical characteristics and the initial conditions are reported below in Table 2.
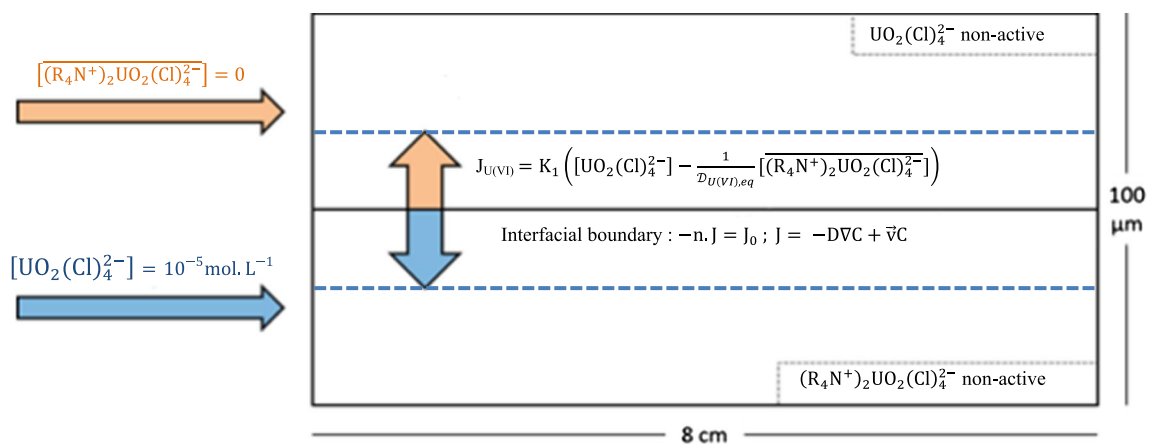

Fig. 2 Representation of the numerical modeling of the mass transfer used in COMSOL Multiphysics® for the chemical system [U(VI)] = 10^{-5} mol L^{-1}, [HCl] = 5 mol L^{-1}, [Aliquat® 336] = 10^{-2} mol L^{-1}, in *n*-dodecane modified with 1-decanol 1 % ($V_a \approx V_o$)
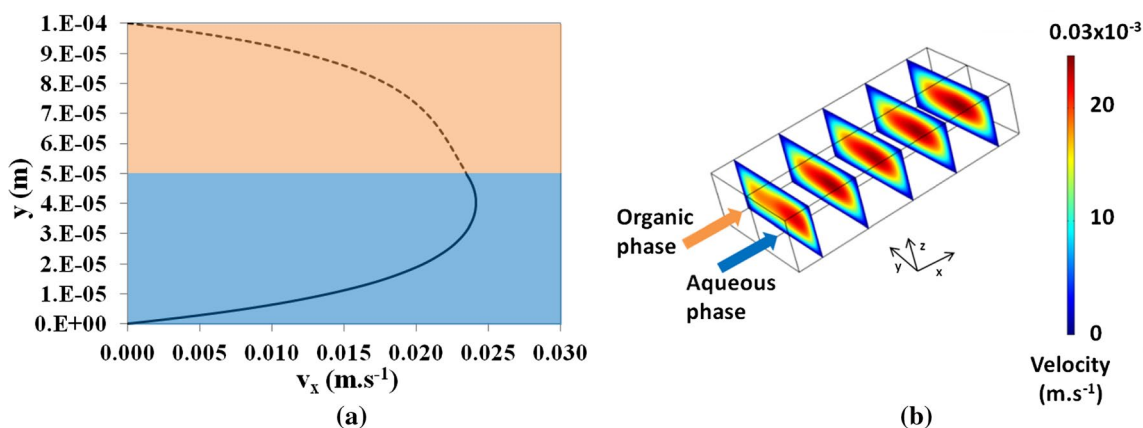
Fig. 3 Velocity profiles modeled by COMSOL Multiphysics® in the microsystem ICC-DY10 of the aqueous and organic phases: Aqueous phase [U(VI)] = 10^{-5} M, [HCl] = 5 mol L^{-1} with Q_a = 0.10 mL h^{-1} (*solid line*), Organic phase [Aliquat® 336] = 10^{-2} mol L^{-1}, *n*-dodecane modified with 1-decanol 1 % (*v*). Q_o = 0.08 mL h^{-1} (*dotted lines*) with h = 50 µm **a** in the plane (x0y) and **b** in 3D

The limit conditions are described in Table 3, and the mass transfer modeling is schematized in Fig. 2.

5 Results and discussion

5.1 Velocity profiles analysis

In this section, the velocity profiles of the organic and aqueous phases are determined numerically for the two chemical systems, and compared with the results obtained with an analytical model. Numerical calculation required a prior optimization of the meshing described in online resource. The representativeness of the calculations made locally in the whole microchannel for the hydrodynamics of stationary flows was verified (see online resource).

5.1.1 System U(VI)/Aliquat® 336

For the system U(VI)/Aliquat® 336, the physical properties enable to apply a flow rate ratio close to 1, allowing for parallel flows and a liquid–liquid interface centered in the microsystem. Therefore, the hydrodynamics modeling has only been done in the geometry of reference ICC-DY10 (Fig. 1). Velocity profiles of the aqueous and organic phases are represented in the plane (x0y) in Fig. 3a and in 3D in Fig. 3b, respectively, for the optimal flow rates Q_a = 0.10 mL h^{-1} and Q_o = 0.08 mL h^{-1}. The maximum velocities of the two phases are very close and located almost exactly at that of the interface. Thus, $v_{a,max}$ = 0.024 m s^{-1} for y = 40 µm and $v_{o,max}$ = 0.023 m s^{-1} for y = h = 50 µm are obtained. Furthermore, we observed that the velocities are relatively low whatever the phase considered. These hydrodynamic

characteristics of the chemical system U(VI)/Aliquat® 336 in the microsystem ICC-DY10 constitute favorable conditions for liquid–liquid extraction as sufficient time is allowed for the extraction reaction to take place.

5.1.2 System Eu(III)/DMDBTDMA

In the case of the system Eu(III)/DMDBTDMA, we determined the best extraction efficiency % E_{Eu} = 26.2 ± 0.9 to know the optimal flow rates Q_a = 0.50 mL h^{-1} and Q_o = 0.03 mL h^{-1}.

As a first step, the modeling was conducted in the microsystem ICC-DY10. The velocity profiles of the aqueous and organic phases are represented in the plane (x0y) in Fig. 4a and in 3D in Fig. 4b for the optimal flow rates. The maximum velocities of the two phases are very different, and while the maximum velocity of the organic phase is located at the liquid–liquid interface, the maximum velocity of the aqueous phase is strongly biased. Thus, $v_{a,max}$ = 0.131 m s^{-1} for y = 26 µm and $v_{o,max}$ = 0.021 m s^{-1} for y = h = 50 µm are obtained. For this chemical system, the maximum velocity of the aqueous phase is high compared to that of the organic phase. These hydrodynamic characteristics of the chemical system Eu(III)/DMDBTDMA in the microsystem ICC-DY10 constitute unfavorable conditions for liquid–liquid extraction.

5.1.3 Comparison of the analytical and numerical models

Two techniques for solving the Navier–Stokes equation have been proposed to simulate velocity profiles of biphasic flows in microsystems: an analytical model and a numerical one using COMSOL Multiphysics®. The values of the maximum velocities of the aqueous and organic
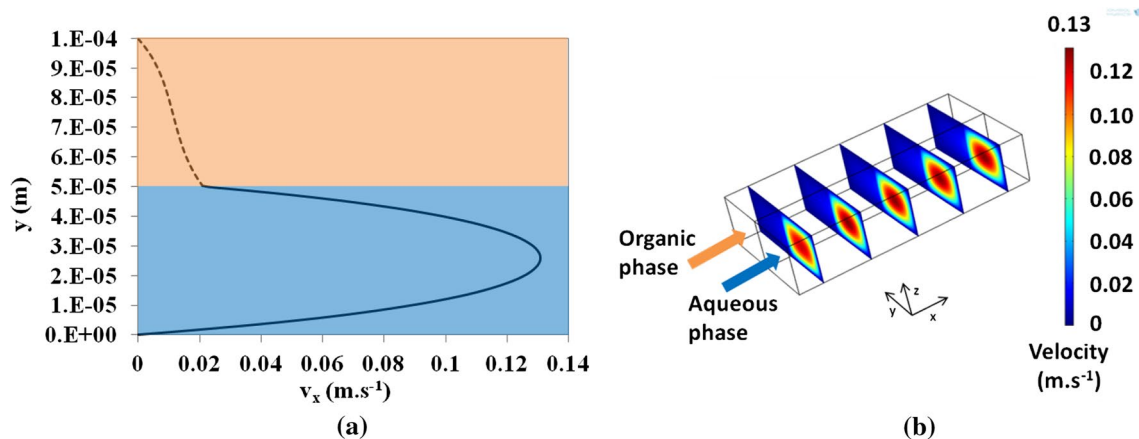
Fig. 4 Velocity profiles modeled by COMSOL Multiphysics® in the microsystem ICC-DY10 of the aqueous and organic phases: Aqueous phase [Eu(III)] = 10^{-2} mol L^{-1}, [HNO$_3$] = 4 mol L^{-1} with Q_a = 0.50 mL h^{-1} (*solid line*), Organic phase [DMDBT-DMA] = 1 mol L^{-1} in *n*-dodecane with Q_o = 0.03 mL h^{-1} (*dotted lines*) with h = 50 µm **a** in the plane (x0y) and **b** in 3D

Table 4 Maximum velocities determined analytically and numerically for the two chemical systems

	U/Aliquat 336®					Eu/DMDBTDMA				
	$v_{a,max}$ (m s^{-1})	$y_{a,max}$ (µm)	$v_{o,max}$ (m s^{-1})	$y_{o,max}$ (µm)	h (µm)	$v_{a,max}$ (m s^{-1})	$y_{a,max}$ (µm)	$v_{o,max}$ (m s^{-1})	$y_{o,max}$ (µm)	h (µm)
Analytical modeling	1.9×10^{-2}	50	1.9×10^{-2}	50	50	5.7×10^{-2}	30	1.7×10^{-2}	56	56
Numerical modeling	2.4×10^{-2}	40	2.3×10^{-2}	50	50	1.31×10^{-2}	26	2.1×10^{-2}	50	50

phases obtained for the two chemical systems are reported in Table 4 for the two models. For the system U(VI)/Aliquat® 336, the values of the maximum velocities of the two phases are close enough, and whatever the model considered, it can be seen that $v_{a,max} \approx v_{o,max}$. Thus, for this chemical system, the two models are consistent. On the other hand, for the system Eu(III)/DMDBTDMA, the values of the maximum velocities of the aqueous phase are very different between the analytical and numerical models. This is less pronounced for the organic phase which flows much more slowly. For this chemical system, the differences can be explained by the fact that the analytical model calculated in the plane (x0y) does not include the microchannel depth (W = 40 µm), and therefore, the interactions related to this third dimension. In addition, the position of the interface has been set by default as the center of the microchannel (h = 50 µm), a rough approximation for this chemical system as in reality its interface is slightly off-centered. This approximation was made as a result of the difficulty that comes with the modeling of a mobile interface, depending on both viscosities and applied flow rates.

5.2 Designing the cross-sectional area of the microchannel

For the chemical system Eu(III)/DMDBTDMA and regardless of the model concerned, the maximum velocity of the aqueous phase is too high relative to that of the organic phase. This suggests that the microchannel geometry is not suitable for this chemical system. Therefore, taking into account the imposed chemical compositions of the two phases, we tried to adapt the microchannel geometry by restricting the flow of the organic phase in a narrowed part of the microchannel in such a way that it occupies only half of the channel to drain the aqueous phase at a lower velocity. Inspired by the geometries described in the literature (Smirnova et al. 2006; Ban et al. 2011), the velocity profiles have been determined for an asymmetric microchannel (Fig. 5) with different depths for the aqueous W_a and organic W_o phases, while keeping flow rates experimentally determined.

We have calculated the velocity profiles for different depths of the microchannel for both the aqueous W_a and organic phases W_o. The specifications of the geometries tested for the optimization of the design of the

microchannel for the Eu/DMDBTDMA system are detailed in Table 5, with the other physical parameters of the phases and the initial conditions.
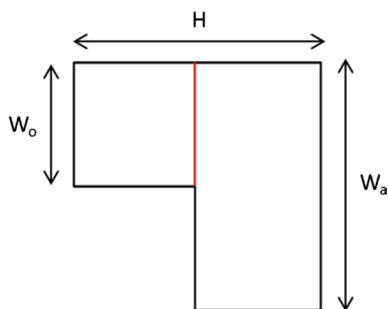

Fig. 5 Microchannel cross section (plane y0z) with an asymmetric geometry. The *red line* stands for the position of the interface which is constant for all the geometries

Velocity profiles obtained are represented in Fig. 6a for geometries 1–4 and in Fig. 6b for geometries 4–7. In Fig. 6a, we note that for a fixed aqueous phase microchannel depth ($W_a = 40$ μm), the velocities of the two phases decrease when the organic phase microchannel depth decreases (W_o ranging from 40 to 10 μm), reaching $v_{a,max} = 6.8$ cm s^{-1} for $W_{org} = 10$ μm. On the contrary, one can choose to reduce the constrain on the aqueous phase by increasing W_a while maintaining constant W_{org}. In Fig. 6b, we note that for a fixed organic phase microchannel depth ($W_o = 40$ μm), the velocities of both phases decrease and the aqueous phase microchannel depth increases (from 40 to 240 μm), leading to $v_{a,max} = 1.5$ cm s^{-1} for $W_a = 240$ μm.

We can observe that whatever the geometry, the position of the maximum velocity in the microchannel on the axis y does not vary: for the aqueous phase, the maximum

Table 5 Initial conditions and parameters for different sections of microsystem geometries tested the numerical computation for the aqueous and organic phases: Aqueous phase [Eu(III)] = 10^{-2} M, [HNO$_3$] = 4 mol L^{-1} with $Q_a = 0.50$ mL h^{-1}, Organic phase [DMDBTDMA] = 1 mol L^{-1} in n-dodecane with $Q_o = 0.03$ mL h^{-1}

|	#1	#2	#3	#4	#5	#6	#7
Q_o (mL h^{-1})				0.03			
Q_a (mL h^{-1})				0.50			
L (mm)				200			
H (μm)				100			
W_o (μm)	10	20	30	40	40	40	40
W_a (μm)	40	40	40	40	80	160	240
$v_{0,o}$ (m s^{-1})	1.67×10^{-2}	0.83×10^{-2}	0.56×10^{-2}	0.42×10^{-2}	0.42×10^{-2}	0.42×10^{-2}	0.42×10^{-2}
$v_{0,a}$ (m s^{-1})	6.94×10^{-2}	6.94×10^{-2}	$\times 10^{-2}$	6.94×10^{-2}	3.47×10^{-2}	1.74×10^{-2}	1.16×10^{-2}
$v_{a,max}$ (m s^{-1})	6.80×10^{-2}	1.10×10^{-2}	1.30×10^{-2}	1.30×10^{-2}	5.90×10^{-2}	2.40×10^{-2}	1.50×10^{-2}
$v_{o,max}$ (m s^{-1})	0.26×10^{-2}	0.83×10^{-2}	1.50×10^{-2}	0.21×10^{-2}	0.76×10^{-2}	0.31×10^{-2}	0.20×10^{-2}
$v_{a,max}/v_{o,max}$	26.2	13.3	8.7	6.20	7.80	7.70	7.50
$A' = A/V$ (m^{-1})	4000	6667	8571	10,000	6667	4000	2857

(a)

(b)
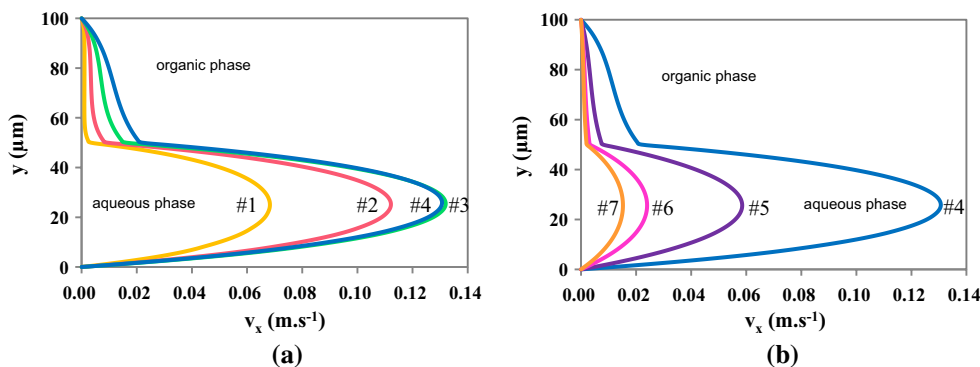
Fig. 6 Velocity profiles for geometries described in Table 6: #1 *yellow*, #2 *red*, #3 *green*, #4 *blue* #5 *purple*, #6 *pink* and #7 *orange* for the aqueous and organic phases: Aqueous phase [Eu(III)] = 10^{-2} mol L^{-1}, [HNO$_3$] = 4 mol L^{-1} with $Q_a = 0.50$ mL h^{-1}, Organic phase [DMDBTDMA] = 1 mol L^{-1} in n-dodecane with $Q_o = 0.03$ mL h^{-1}

velocity is located at $y = 26$ µm, and for the organic phase, the maximum velocity is located at the interface $y = h = 50$ µm.

These results confirm the interest to constrain the organic phase in a restricted part of the microchannel in order to reduce the velocity of the aqueous phase by increasing the depth of the microchannel part dedicated to the aqueous phase.

The reduction in the maximum velocity of the aqueous phase is not the only criterion to be considered because the modification of the geometry leads to a variation in the specific interfacial area. Indeed, the lowest velocities are obtained for $W_a = 240$ µm and $W_o = 40$ µm (geometry #7), i.e., when the dimensions of the microchannel part for the aqueous phase increase by comparison with the geometry of reference. Nevertheless, for this geometry, the specific interfacial area is considerably reduced due to the important increase in the aqueous phase volume with a constant interfacial area. This criterion is unfavorable for obtaining good extraction performance.

Thanks to the modeling, we have shown that the optimization of the geometry of a microsystem dedicated to the liquid–liquid extraction considering a centered interface requires that one:

- determines the viscosities of the two phases,
- imposes $W_a/W_o \approx \mu_o/\mu_a$ to have similar maximum velocities for the two phases in an asymmetric microchannel.

5.3 Validation of the mass transfer modeling for the extraction of U(VI)

As described in Sect. 4.1, the kinetic law which is used for the mass transfer modeling for the system U(VI)/Aliquat® 336 is described by Eq. (7). Nevertheless, to use this equation, the value of the forward global transfer coefficient constant K_1 should be estimated. To do so, we introduced different values of K_1 into the model for the microsystem of 8 cm and calculated the extraction efficiencies through the modeling, each time. Then, the calculated values are compared with the experimental value of the extraction efficiency for $L = 8$ cm as shown in Fig. 7.

These results show that a constant K_1 estimated at $(1.6 \pm 0.2) \times 10^{-5}$ m s^{-1}, taking into account measurement uncertainty, and leads to an extraction efficiency in good agreement with the one experimentally obtained $\%E_{U(VI),th} = \%E_{U(VI),exp} = (76.3 \pm 6.5)$ %. To validate the K_1 value, the three experimental results are compared with 6 theoretical results obtained by the numerical modeling using the determined forward global transfer coefficient K_1 for different microchannel lengths. They are presented in Fig. 8.
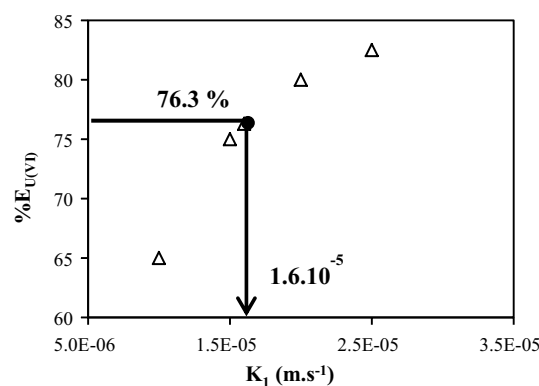

Fig. 7 Estimation of K_1 (calculated values *triangle*, experimental value *filled circle*) for the system [U(VI)] = 10^{-5} mol L^{-1}, [HCl] = 5 mol L^{-1}, [Aliquat® 336] = 10^{-2} mol L^{-1} in *n*-dodecane modified with 1-decanol 1 % (v) with $Q_a = 0.10$ mL h^{-1} and $Q_o = 0.08$ mL h^{-1}, $L = 8$ cm, $H = 100$ µm
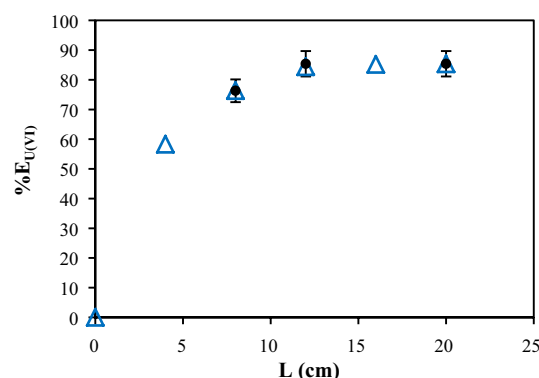

Fig. 8 Comparison of the experimental (*circle*) and theoretical (*triangle*) results for the extraction efficiency as a function of the microchannel length for the system [U(VI)] = 10^{-5} mol L^{-1}, [HCl] = 5 M, [Aliquat® 336] = 10^{-2} mol L^{-1} in *n*-dodecane modified with 1-decanol 1 % (v) with $Q_a = 0.10$ and $Q_o = 0.08$ mL h^{-1}

The experimental and theoretical results are in agreement. Therefore, this value of global transfer coefficient is kept for the mass transfer modeling in the microsystem. The concentration profiles of $[UO_2(Cl)_4^{2-}]$ and $[(R_4N^+)_2UO_2(Cl)_4^{2-}]$ given by the modeling are shown in Fig. 9a, b, respectively. We can see that the concentration of $UO_2(Cl)_4^{2-}$ decreases along the microchannel on the *x*-axis, while as in the contrary, the concentration of $(R_4N^+)_2UO_2(Cl)_4^{2-}$ increases along the microchannel. Moreover, the concentration profiles are not uniform in the width for each phase. In particular, for the organic phase, $[(R_4N^+)_2UO_2(Cl)_4^{2-}]$ is logically higher near the interface than near the opposite wall of the microchannel. This effect is due to the fact that the complex of U(VI) with Aliquat® 336 is created at the interface and then diffuses over time
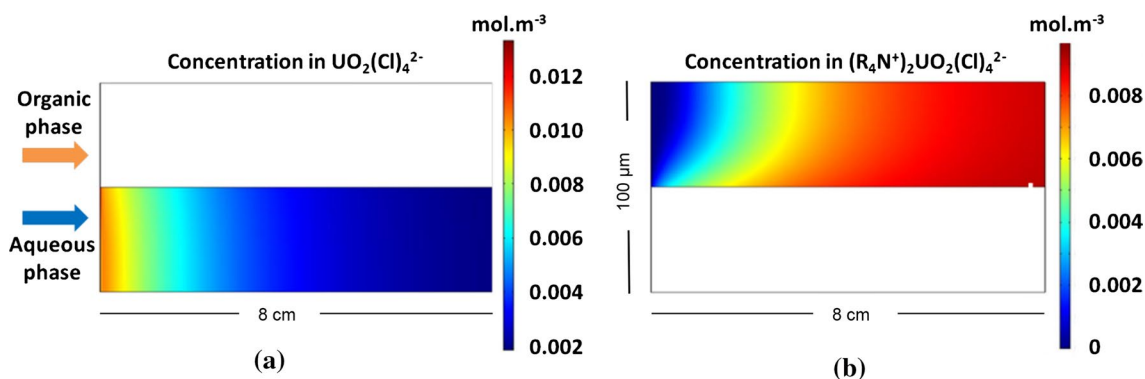
Fig. 9 Numerical modeling in the plane x0y of a microsystem ICC-DY10 ($L = 8$ cm, H = 100 μm) for the chemical system [U(VI)] = 10^{-5} mol L^{-1}, [HCl] = 5 mol L^{-1}, [Aliquat$^®$ 336] = 10^{-2} mol L^{-1} in n-dodecane modified with 1-decanol 1 % (v) with $Q_a = 0.10$ and $Q_o = 0.08$ mL h^{-1} **a** concentration in UO$_2$(Cl)$_4^{2-}$ and **b** concentration in (R$_4$N$^+$)$_2$UO$_2$(Cl)$_4^{2-}$

into the organic phase. Moreover, this modeling allows to determine the optimal channel length to achieve the optimal extraction performances. Here, the optimal length is $L_{opt} \approx 12$ cm for the chemical system U(VI)/Aliquat$^®$ 336 (Fig. 8).

6 Conclusion

Thanks to the simplified Navier–Stokes equation applied to the biphasic microflow, analytical and numerical modeling of the hydrodynamics has been proposed for two chemical systems. Comparison of the results allowed to highlight the limitations of the analytical model which does not take into account the depth of the microchannel ($W = 40$ μm) and therefore the third dimension-related interactions. However, the comparison of analytical and numerical results has helped to validate the numerical model. Following its validation, the numerical resolution, more rigorous, has been used to bring ways of optimization of the hydrodynamics for Eu(III)/DMDBTDMA system for which viscosities ratio is far from 1.

A modeling of mass transfer was developed in the case of the extraction of uranium(VI) from 5 mol L^{-1} HCl by Aliquat$^®$ 336. A chemical anion-exchange reaction occurring at the interface was taken into account and been integrated the model which involves a forward global transfer coefficient K_1 and a backward global transfer coefficient K_{-1}. The ratio K_1/K_{-1} was deduced from equilibrium data, and the value of K_1 was determined by a process of trial-and-error modeling ($K_1 = (1.6 \pm 0.2) \, 10^{-5}$ m s^{-1}).

In this study, the modeling of mass transfer was coupled with the modeling of hydrodynamics. The results obtained by numerical computation are quite consistent with the experimental results for the studied chemical system (U(VI)/Aliquat$^®$ 336) and different lengths of

microchannel ($L = 8$, 12 and 20). These results allow validating the model of hydrodynamics/mass transfer coupling developed.

From the point of view of prototyping, the mass transfer modeling allows defining the final geometric feature that was missing, namely the optimal length of the microchannel for maximum yield of extraction.

References

Albers A, Marz J, Burkardt N (2003) DS 31: Proceedings of ICED 03, the 14th international conference on engineering design, Stockholm, Sweden, pp 25–26

Aota A, Hibara A, Kitamori T (2007) Pressure balance at the liquid-liquid interface of micro countercurrent flows in microchips. Anal Chem 79:3919–3924

Ban Y, Kikutani Y, Tokeshi M, Morita Y (2011) Extraction of Am(III) at the interface of organic-aqueous two-layer flow in a microchannel. J Nucl Sci Technol 48(10):1313–1318

Barbano PG, Rigali L (1978) Spectrophotometric determination of uranium in sea water after extraction with Aliquat-336. Anal Chim Acta 96(1):199–201

Bendsøe MP, Sigmund O (2003) Topology optimization: theory, methods and applications. Springer, Berlin

Bird RB, Stewart WE, Lightfoot EN (2007) Transport phenomena. Wiley, New York

Bose P, Albonesi DH, Marculescu D (2003) Guest editors' Introduction: power and complexity aware design. IEEE Micro 23(8):8–11

Brennich ME, Koster S (2014) Tracking reactions in microflow. Microfluid Nanofluid 16:39–45

Cherlo S, Kariveti KS, Pushpavanam S (2010) Experimental and numerical investigations of two-phase (liquid-liquid) flow behavior in rectangular microchannels. Ind Eng Chem Res 49:893–899

Ciceri D, Mason L, Harvie D, Perera J, Stevens G (2013) Modelling of interfacial mass transfer in microfluidic solvent extraction: part II. Heterogeneous transport with chemical reaction. Microfluid Nanofluid 14:213–224

Ciceri D, Perera JM, Stevens GW (2014) The use of microfluidic devices in solvent extraction. J Chem Technol Biotechnol 89:771–786

Duffy D, Mc Donald J, Schueller O, Whitesides G (1998) Rapid prototyping of microfluidic systems in poly(dimethylsiloxane). Anal Chem 70:4974–4984

Erickson D (2005) Towards numerical prototyping of labs-on-chip: modeling for integrated microfluidic devices. Microfluid Nanofluid 1:301–318

Erickson D, Li D (2004) Integrated microfluidic devices. Anal Chim Acta 507:11–26

Fodor PS, D'Alessandro J (2011) Improving fuel usage in microchannel based fuel cells. Comsol conference, Boston

Gervais T, Jensen KF (2006) Mass transport and surface reactions in microfluidic systems. Chem Eng Sci 61:1102–1121

Goyal S, Desai AV, Lewis RW, Ranganathan DR, Li H, Zeng D, Reichert DE, Kenis PJA (2014) Thiolene and SIFEL-based microfluidic platforms for liquid–liquid extraction. Sens Actuators B 190:634–644

Hellé G, Mariet C, Cote G (2012) Microfluidic tools for the liquid-liquid extraction of radionuclides in analytical procedures. Procedia Chem 7:679–684

Hellé G, Mariet C, Cote G (2014) Liquid-liquid microflow patterns and mass transfer of radionuclides in the systems Eu(III)/HNO$_3$/DMDBTDMA and U(VI)/HCl/Aliquat® 336. Microfluid Nanofluid 17(6):1113–1128

Hellé G, Mariet C, Cote G (2015) Liquid–liquid extraction of uranium(VI) with Aliquat 336 from HCl media in microfluidic devices: combination of micro-unit operations and online ICP-MS determination. Talanta 139:123–131

Hisamoto H, Shimizu Y, Uchiyama K, Tokeshi M, Kikutani Y, Hibara A, Kitamori T (2003) Chemicofunctional membrane for integrated chemical processes on a microchip. Anal Chem 75:350–354

Hotokezaka H, Tokeshi M, Harada M, Kitamori T, Ikeda Y (2005) Development of the innovative nuclide separation system for high-level radioactive waste using microchannel chip- extraction behavior of metal ions from aqueous phase to organic phase in microchannel. Prog Nucl Energy 47(1–4):439–447

Jha MK, Kumar V, Singh RJ (2002) Solvent extraction of zinc from chloride solutions. Solvent Extr Ion Exch 20(3):389–405

Jovanovic J (2011) Liquid-liquid microreactors for phase transfer catalysis. Phd, Université d'Eindhoven

Kashid MN, Kowalinski W, Renken A, Baldyga J, Kiwi-Minsker L (2012) Analytical method to predict two-phase flow pattern in horizontal micro-capillaries. Chem Eng Sci 74:219–232

Krishnamoorthy S, Feng J, Henry AC, Locascio LE, Hickman JJ, Sundaram S (2006) Simulation and experimental characterization of electroosmotic flow in surface modified channels. Microfluid Nanofluid 2(4):345–355

Kubota F, Uchida JI, Goto M (2003) Extraction and separation of rare earth metals by a microreactor. Solvent Extr. Res. Dev. Jpn 10:93–102

Ladeveze F (2005) Microréacteur en synthèse chimique: rôle de l'hydrodynamique et effets de la miniaturisation. Thesis, Institut National Polytechnique de Toulouse (http://ethesis.inp-toulouse.fr/archive/00000219/01/ladeveze.pdf, 16 June 2015)

Liu M, Novak U, Plazl I, Franko M (2014) Optimization of a thermal lens microscope for detection in a microfluidic chip. Int J Thermophys 35(11):2011–2022

Lubej M, Novak U, Liu M, Martelanc M, Franko M, Plazl I (2015) Microfluidic droplet-based liquid–liquid extraction: online model validation. Lab Chip 15:2233–2239

Malengier B, Pushpavanam S (2012) Comparison of co-current and counter-current flow fields on extraction performance in micro-channels. Adv Chem Eng Sci 2:309–320

Malengier B, Pushpavanam S, D'haeyer S (2011) Optimizing performance of liquid–liquid extraction in stratified flow in micro-channels. J Micromech Microeng. doi:10.1088/0960-1317/21/11/115030

Malengier B, Tamalapakula JL, Pushpavanam S (2012) Comparison of laminar and plug flow-fields on extraction performance in micro-channels. Chem Eng Sci 83:2–11

Manz A, Eijkel JCT (2001) Miniaturization and chip technology. What can we expect? Pure Appl Chem 73(10):1555–1561

Maruyama T, Matsushita H, Uchida J-I, Kubota F, Kamiya N, Goto M (2004) Liquid membrane operations in a microfluidic device for selective separation of metal ions. Anal Chem 76:4495–4500

Mason LR, Ciceri D, Harvie DJE, Perera JM, Stevens GW (2013) Modelling of interfacial mass transfer in microfluidic solvent extraction: part I. Heterogenous transport. Microfluid Nanofluid 14:197–212

Mott D, Howell P, Golden J, Kaplan C, Ligler F, Orana E (2006) Toolbox for the design of optimized microfluidic components. Lab Chip 6:540–549

Ng JM, Gitlin I, Stroock A, Whitesides G (2002) Components for integrated poly(dimethylsiloxane) microfluidic systems. Electrophoresis 23(20):3461–3473

Nishihama S, Nishimura G, Hirai T, Komasawa I (2004) Separation and recovery of Cr(VI) from simulated plating waste using microcapsules containing quaternary ammonium salt extractant and phosphoric acid extractant. Ind Eng Chem Res 43:751–757

Nishihama S, Tajiri Y, Yoshizuka K (2006) Separation of lanthanides using micro solvent extraction system. Ars Separatoria Acta 4:18–26

Novak U, Pohar A, Plazl I, Znidarsic-Plazl P (2012) Ionic liquid-based aqueous two-phase extraction within a microchannel system. Sep Purif Technol 97:172–178

Novak U, Lakner M, Plazl I, Znidarsic-Plazl P (2015) Experimental studies and modeling of α-amylase aqueous two-phase extraction within a microfluidic device. Microfluid Nanofluid 19:75–83

Panikowska K, Tiwari A, Alcock J (2009) Design in the microfluidic domain as compared to other domains. In: International conference of engineering design, Standford, (USA) August 24–27

Panikowska K, Tiwari A, Alcock JR (2011) Towards service-orientation-the state of service thoughts in the microfluidic domain. J Adv Manuf Technol 56:135–142

Pohar A, Lakner M, Plazl I (2012) Parallel flow of immiscible liquids in a microreactor: modeling and experimental study. Microfluid Nanofluid 12:307–316

Przekwas AJ, Makhijani VB (2001) Mixed-dimensionality, multi-physics simulation tools for design analysis of microfluidic devices and integrated systems. In: International conference in modeling and simulation of microsystems, www.cr.org, March 19–21

Ranjan V, Kumar A, Prakash G, Mandal R (2012) Effect of geometry of the grooves on the mixing of fluids in micro mixer channel. Comsol conference, Bangalor

Razik A, Ali F, Amia FA (1989) Evaluation of the stability constants of uranyl association complexes with chloride, fluoride, bromide, and sulfate anions in solutions of constant ionic strength. Microchem J 39:258–264

Rieger R, Weiss C, Wigley G, Bart H-J, Marr R (1996) Investigating the process of liquid-liquid extraction by means of computational fluid dynamics. Comput Chem Eng 20(12):1467–1475

Ryan JL (1963) Anion exchange and non-aqueous studies of the anionic chloro complexes of the hexavalent actinides. Inorg Chem 2:348–358

Sato T (1983) Liquid-liquid extraction of rare-earth elements from aqueous acid solutions by acid organophosphorus compounds. Hydrometallurgy 22:121–140

Smirnova A, Mawatari K, Hibara A, Proskurnin MA, Kitamori T (2006) Micro-multiphase laminar flows for the extraction and detection of carbaryl derivative. Anal Chim Acta 558:69–74

Soderholm L, Skanthakumar S, Wilson R (2011) Structural correspondence between uranyl chloride complexes in solution and their stability constants. J Phys Chem 115:4959–4967

Song H, Wang Y, Pant K (2012) Cross-stream diffusion under pressure-driven flow in microchannels with arbitrary aspect ratios: a phase diagram study using a three-dimensional analytical model. Microfluid Nanofluid 12:265–277

Squires TM, Quake SR (2005) Microfluidics: fluid physics at the nanoliter scale. Rev Mod Phys 77(3):977–1026

Stiles PJ, Fletcher DF (2004) Hydrodynamic control of the interface between two liquids flowing through a horizontal or vertical microchannel. Lab Chip 4:121–124

Tay FE (2002) Microfluidics and bioMEMS applications. Kluwer, Boston

Tokeshi M, Kitamori T (2005) Continuous flow chemical processing on a microchip using operations and a multiphase flow network. Prog Nucl Energy 47(1–4):434–438

Tokeshi M, Minagawa T, Kitamori T (2000) Integration of a micro-extraction system on a glass chip: ion-pair solvent extraction of Fe(II) with 4,7-diphenyl-1,10-phenanthrolinedisulfonic acid and tri-n-octylmethylammonium chloride. Anal Chem 72:1711–1714

Toulemonde V (1995) Cinétique d'extraction liquide-liquide du nitrate d'uranyle et des nitrates d'actinides (III) et des lanthanides (III) par des extractants à fonction amide. Thesis, Paris 6 University, France (http://www.iaea.org/inis/collection/NCLCollectionStore/_Public/29/016/29016270.pdf, 16 June 2015)

Tsaoulidis D, Dore V, Angeli P, Plechkova NV, Seddon KR (2013a) Extraction of dioxouranium(VI) in small channels using ionic liquids. Chem Eng Res Des 91:681–687

Tsaoulidis D, Dore V, Angeli P, Plechkova NV, Seddon KR (2013b) Flow patterns and pressure drop of ionic liquid–water two-phase flows in microchannels. Int J Multiphas Flow 54:1–10

Ungerböck B, Pohar A, Mayr T, Plazl I (2013) Online oxygen measurements inside a microreactor with modeling of transport phenomena. Microfluid Nanofluid 14(3):565–574

Vilkner T, Janasek D, Manz A (2004) Micro total analysis systems. Recent developments. Anal Chem 76:3373–3386

Wang X, Hirano H, Xie G, Xu D (2013) VOF modeling and analysis of the segmented flow in Y-shaped microchannels for microreactor systems. Adv High Energy Phys. doi:10.1155/2013/732682

Whitesides G (2006) The origins and the future of microfluidics. Nature 442(7101):368–373

Wootton R, Fortt R, DeMello AJ (2002) A microfabricated nanoreactor for safe. Org Process Res Dev 6:187–189

Xu J, Paimin R, Wei S, Xungai W (2003) Investigation of solubility of aliquat 336 in different extracted solutions. Fiber Polym 4(1):27–31

Zhao Y, Chen G, Yuan Q (2006) Liquid-liquid two-phase flow patterns in a rectangular microchannel. Am Inst Chem Eng J 52(12):4052–4060

Znidarsic-Plazl P, Plazl I (2007) Steroid extraction in a microchannel system-mathematical modelling and experiments. Lab Chip 7:883–889

Znidarsic-Plazl P, Plazl I (2009) Modelling and experimental studies on lipase-catalyzed isoamyl acetate synthesis in a microreactor. Process Biochem 44:1115–1121